Stretchable, Transparent Graphene Interconnects for Arrays of Microscale Inorganic Light Emitting Diodes on Rubber Substrates

Rak-Hwan Kim,[†,∇] Myung-Ho Bae,[‡,∇] Dae Gon Kim,[†] Huanyu Cheng,[§] Bong Hoon Kim,[†,‖] Dae-Hyeong Kim,[†] Ming Li,[§,⊥] Jian Wu,[§] Frank Du,[†] Hoon-Sik Kim,[†] Stanley Kim,[†,‡] David Estrada,[‡] Suck Won Hong,[#] Yonggang Huang,[§] Eric Pop,[‡] and John A. Rogers[*,†]

[†]Department of Materials Science and Engineering, Beckman Institute for Advanced Science and Technology and Frederick Seitz Materials Research Laboratory, University of Illinois at Urbana—Champaign, Urbana, Illinois 61801, United States

[‡]Department of Electrical and Computer Engineering, Micro and Nanotechnology Laboratory, University of Illinois at Urbana—Champaign, Urbana, Illinois 61801, United States

[§]Department of Mechanical Engineering and Department of Civil and Environmental Engineering, Northwestern University, Evanston, Illinois 60208, United States

[‖]Department of Materials Science and Engineering, Korea Advanced Institute of Science and Technology (KAIST), Daejeon, 305-701, Korea
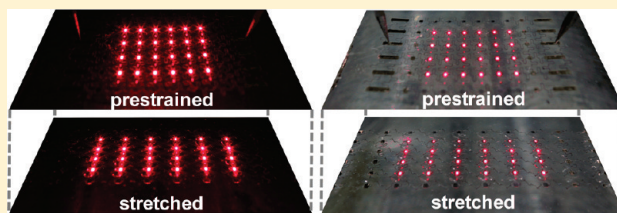
[⊥]State Key Laboratory of Structural Analysis for Industrial Equipment, Dalian University of Technology, Dalian 116024, People's Republic of China

[#]Department of Nanomaterials Engineering, Pusan National University, Miryang, 627-706, Korea

Ⓢ Supporting Information

ABSTRACT: This paper describes the fabrication and design principles for using transparent graphene interconnects in stretchable arrays of microscale inorganic light emitting diodes (LEDs) on rubber substrates. We demonstrate several appealing properties of graphene for this purpose, including its ability to spontaneously conform to significant surface topography, in a manner that yields effective contacts even to deep, recessed device regions. Mechanics modeling reveals the fundamental aspects of this process, as well as the use of the same layers of graphene for interconnects designed to accommodate strains of 100% or more, in a completely reversible fashion. These attributes are compatible with conventional thin film processing and can yield high-performance devices in transparent layouts. Graphene interconnects possess attractive features for both existing and emerging applications of LEDs in information display, biomedical systems, and other environments.

KEYWORDS: Microscale LEDs, graphene, transparent, stretchable interconnects

The excellent mechanical, thermal, and electronic properties of graphene have motivated wide-ranging scientific and engineering studies.[1] Recent advances in synthesis and processing[2] have created interest in practical applications as robust, transparent conductors for touch screens, photovoltaic cells, and light-emitting diodes (LEDs). In these systems, graphene could serve as an attractive substitute to more traditional materials such as TCOs (transparent conducting oxides), due to its favorable mechanical properties and its potential to reduce costs. Recently, such uses of graphene have been reported by many groups, including possibilities for use in organic and inorganic LEDs.[3−6] Previous results are limited, however, to single pixel demonstrations, in modes that do not fully exploit the unique mechanics afforded by graphene compared to TCOs. Further process developments and alternative strategies are needed for interconnected arrays of LEDs, and for applications of graphene in unusual areas such as stretchable electronics and optoelectronics. In this work, we explore the use of graphene as a stretchable,

transparent electrode and interconnect for microscale inorganic LEDs (i.e., μ-ILEDs) in a manner that exploits its extremely low flexural rigidity to enable conformal contacts to structures that present significant surface relief. When configured into serpentine geometries, graphene provides robust interconnects for stretchable μ-ILED arrays, where reversible, linear elastic behavior is observed for strains exceeding 100%. Device demonstrations and detailed examination of the materials and mechanics aspects highlight some appealing features of graphene used in this manner.

Figure 1a schematically illustrates our key process steps for fabricating μ-ILEDs (p-GaAs/p-AlGaAs/p-InAlP/quantum well (AlGaInP/InGaP/AlGaInP)/n-InAlP/n-AlGaAs/n-GaAs) with transparent graphene electrodes. First, graphene is grown by
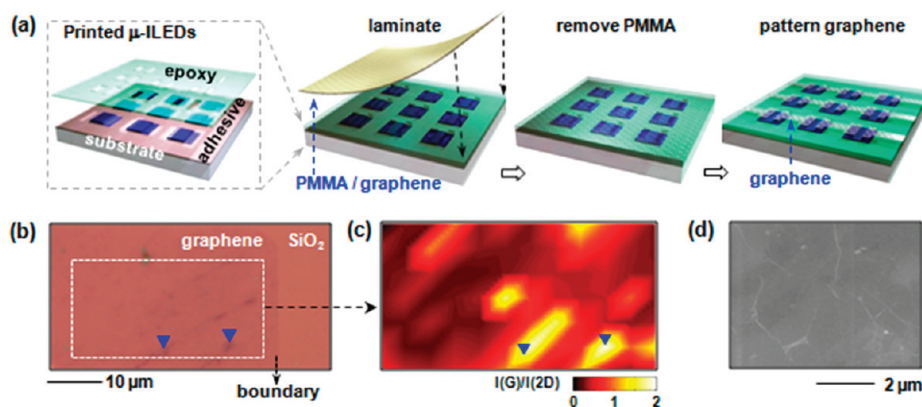
Figure 1. (a) Schematic illustration of layouts and fabrication procedures for μ-ILEDs with transparent graphene electrodes. (b) Optical image of a graphene film transferred to a SiO_2/Si substrate. The boundary (dashed arrow) indicates the patterned edge of the graphene film. (c) Raman map of $I(G)/I(2D)$ ratio from the region indicated by the dashed white box in the microscope image of frame b. (d) Typical scanning electron microscopy (SEM) image of the transferred graphene film.

chemical vapor deposition $(CVD)^2$ on sheets of copper foil, with temperatures, pressures, and gas mixtures of 1000 °C, 2.6 Torr, and $CH_4:H_2$ (850:50 sccm), respectively. Removing the graphene by coating it with a thin layer of poly(methyl methacrylate) (PMMA A2; Microchem.; 100 nm thick) and then etching away the copper (1 M aqueous solution of $FeCl_3$), followed by transfer completes the integration (See Supporting Information and Figure S1). The receiving substrate consists of a printed array of AlInGaP μ-ILEDs ($100 \times 100 \ \mu m^2$; 2.5 μm thickness), formed and processed according to procedures described elsewhere.[7] These devices support predefined Ohmic metal n-contacts and etched regions for p-contacts. A spin-coated thin dielectric layer (epoxy; Microchem.; SU-8; 1.2 μm thickness), patterned to expose both contacts, encapsulates all other parts of the structure, as shown in the schematic illustration of Figure 1a (boxed image). Washing away the PMMA with acetone and then gently drying leads to spontaneous mechanical sagging of the graphene, in a manner that establishes conformal coverage over the relief associated with the μ-ILEDs and their dielectric overcoats. Photolithography and reactive ion etching patterns the graphene into interconnect structures, thereby completing the fabrication (right frame of Figure 1a).

To characterize the typical CVD graphene employed in this study, we present an optical image of graphene transferred to a 300 nm thick layer of SiO_2 on a Si substrate (Figure 1b). This image displays uniform contrast, except for some isolated dark regions, indicated by blue triangles. Raman spectroscopy (633 nm excitation) over a representative area (dashed white box in Figure 1b) yields a map of the ratio of peak intensities in the G and 2D bands, $I(G)/I(2D)$, as shown in Figure 1c (pixel size $\sim$3 μm; beam diameter $\sim$1 μm). Most areas have ratios $I(G)/I(2D) < 0.5$, consistent with monolayer graphene.[8,9] The small regions with dark contrast (blue triangles) correspond to ratios of $\sim$1.5 (Figure 1c) which are a few graphitic islands. The SEM image in Figure 1d also shows expected rippled structures (white) in the transferred graphene film, created due to mismatches in the thermal expansion coefficients of copper and graphene.[10]

A key feature of the graphene as implemented here is its ability to conform to significant surface topography. This behavior results from its exceptionally low flexural rigidity, EI $\sim 1.1 \times 10^{-19}$ J (per unit width) for monolayer graphene,[11] which is 6

orders of magnitude smaller than that of PMMA (100 nm thick, elastic modulus 2.89 GPa).[12] The resulting contact (i.e., intimate, conformal lamination) provides robust electrical interconnects between devices, even for cases where the associated relief is significant, as illustrated schematically in Figure 2a. Step heights from the top of the epoxy layer to the surfaces of the p- and n-contact regions are $\sim$1.2 and $\sim$3 μm, respectively. Surface profilometry measurements (Sloan Dektak) and optical micrographs at different stages of the process flow appear in panels b and c of Figure 2, respectively. These results show that, after removal of the PMMA, the graphene conforms nearly perfectly to the underlying relief structures, as will be further demonstrated in Figure 3. The mechanism relies on low flexural rigidity of graphene, which can lead to the bending energy that is much smaller than the adhesion energy associated with contact to the GaAs, even for substantial relief heights. Mechanics analysis detailed in the Supporting Information shows that sagging of graphene onto GaAs occurs when

$$\frac{9EIh^2}{\gamma L^4} < 0.01 \qquad (1)$$

where EI is the flexural rigidity (per unit width), h is the total height of the relief (sum of step height of p (or n) contact region(s) and the thickness of epoxy layer), L is the step length, and γ is the work of adhesion between graphene and GaAs (per unit width). For EI = 1.1×10^{-19} J (graphene), $h = 3 \ \mu$m as in experiments, and $\gamma \sim 0.15$ J/m^2 (ref 13), a step length L as small as a few micrometers still ensures sagging. The percentage of contact coverage between graphene and GaAs is given analytically by $1 - 2[18EIh^2/(\gamma L^4)]^{1/4}$, and is shown in Figure 2d. For $L = 20 \ \mu$m as in experiments, 99% and 60% of overlying films of graphene and PMMA (100 nm)/graphene, respectively, come into conformal contact (see Supporting Information and Figure S2 for details).

For use of graphene in this manner, the contact resistance, the sheet resistance, and the optical transparency are all important; the last two aspects are the subject of many published studies.[10,14] Low sheet resistance can be achieved either by growing multilayer graphene directly or by creating it through multiple stacking of single layers.[8,14] The latter method is preferred here due to improved control and yield in transfer onto relief features.
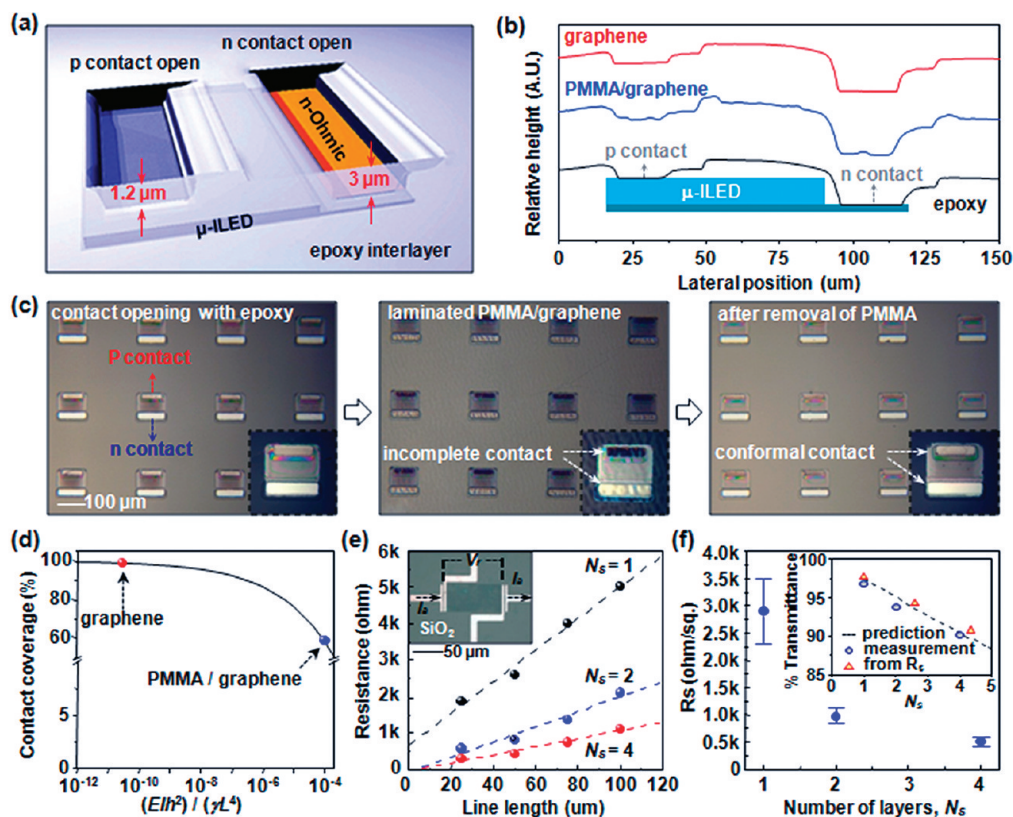
Figure 2. (a) Schematic illustration of μ-ILEDs with thin layers of epoxy interlayer dielectrics showing recessed features at the p and n contacts. (b) Surface profiles of the device regions at different stages of the fabrication: bottom, contact regions exposed through a thin layer of epoxy; middle, laminated with a thin bilayer of PMMA/graphene; top, after removing the PMMA. The illustration at the bottom shows the corresponding layout of the μ-ILED device. (c) Optical images of μ-ILEDs at different stages corresponding to the data of frame b. Insets provide magnified views of individual devices. (d) Scaling of the contact coverage as a function of a dimensionless combination of flexural rigidity EI, total height of the underlying relief h, width of the p (or n) contact region(s) L, and work of adhesion γ. (e) Resistance of films with different numbers of transferred graphene layers ($N_S = 1$, 2, and 4) as a function of four channel lengths. The inset provides an optical image of the four-probe geometry on patterned graphene. (f) Sheet resistance of films (R_S) as a function of N_S, averaged over each of the four data points from (e). The inset provides predicted (dashed line), calculated (triangles), and measured (circles) transmittances of graphene films with different numbers of layers, at a wavelength of 670 nm.

To evaluate properties of stacked films after transfer of different numbers of layers (N_S), Raman spectroscopy was performed for $N_S = 1$, 2, and 4 as shown in Figure S3a in the Supporting Information. The results are consistent with a recent report by Bae et al.[10] suggesting that physical properties of monolayer graphene persist in such stacks, unlike the behavior of exfoliated multilayers, where the mobility decreases with increasing layer number (see Supporting Information for details).[9]

To examine the electrical characteristics of graphene films and to establish their suitability for use as interconnects, we fabricated four-probe geometries with various widths (W) and lengths (L), defined by photolithography and etching. Here, contacts consist of a bilayer of Ti (2 nm)/Au (40 nm), as shown in the inset of Figure 2e. Current flows through the two outer electrodes (I_a), and the voltage drop is measured across the inner two electrodes (V_r) as indicated by labels in the inset. Figure 2e presents the resistance as a function of channel length for $N_S = 1$, 2, and 4 with $W = 50$ μm. For each case, the resistance linearly increases with channel length. The slopes of the linear region indicate that the resistance per unit length (for the given W) decreases monotonically from ~43.3 Ω/μm for $N_S = 1$ to ~20.8 Ω/μm for $N_S = 2$ and to ~11.2 Ω/μm for $N_S = 4$, thereby illustrating the ability to scale the resistances into ranges needed

for practical use. The corresponding sheet resistance, R_S, as a function of N_S appears in Figure 2f. The results suggest that R_S decreases by as much as a factor of 5 as N_S increases from 1 to 4, which is lower than expected based on simple considerations but is consistent with previous reports.[10,14] Possible explanations of this behavior could be due to upper layers of graphene bridging cracks in underlying layers or due to an increase in the charge carrier concentration after multiple transfers caused by intercalated impurities or trapped oxygen and water molecules. Using the dependence of R_S on N_S, it is possible to estimate the variation of optical transmittance, T, with N_S, if we assume that the optical conductivity for Dirac fermions in graphene is a universal constant, $G_{OP} = e^2/4\hbar$ (=6.08×10^{-5} Ω^{-1}), where e and $\hbar$ are the elementary charge and Planck's constant, respectively. In this case, T is also universal, given by $T = (1 + N_S Z_0 G_{OP}/2)^{-2} \approx (1 - 0.025636 N_S)$, where Z_0 (=377 Ω) is the vacuum impedance.[15,16] The value of T predicted in this manner appears in the inset of Figure 2f as a dashed line. To relate an effective N_S to R_S, we define, $N_{Seff} = R_{S1}/R_{SN}$, where R_{SN} is R_S of N-stacked films. By assuming $N_S = N_{Seff}$, we obtain data indicated by triangles in the inset of Figure 2f, consistent with theoretical prediction. Measurements of T at a wavelength of 670 nm, coincident with the emission of our μ-ILEDs, also follow
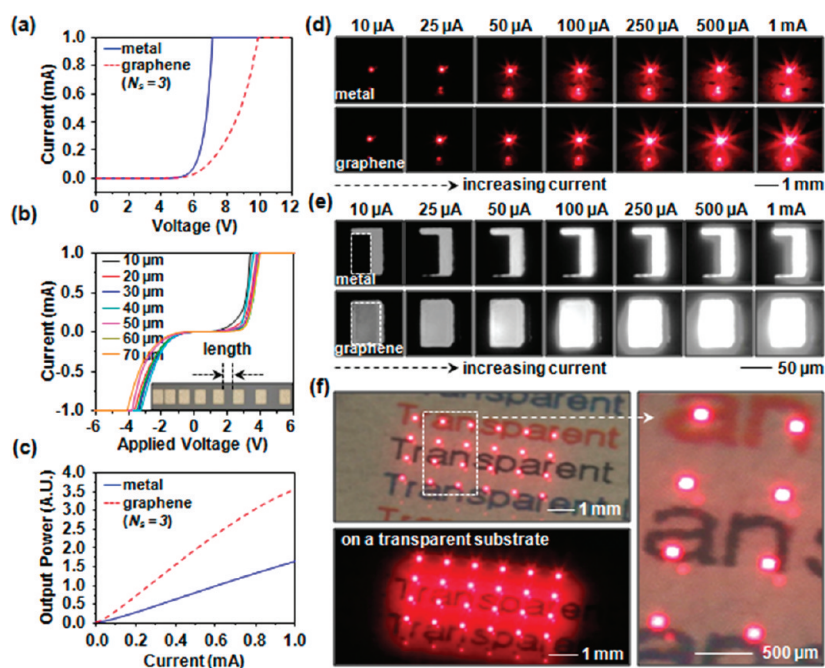
Figure 3. (a) Current−voltage measurements from a single μ-ILED with Ohmic metal contacts (p-contact Pt/Ti/Pt/Au, 10/40/10/50 nm; n-contact Pd/Ge/Au, 5/35/50 nm) and with graphene electrodes and Ohmic contact only for the n-GaAs region, respectively. (b) Current−voltage characteristics evaluated by two-point transmission line method (TLM) to assess the quality of the graphene/p-GaAs contact. The inset provides an image of the test structure used for this measurement. Thin bilayer contacts (Cr/Au, 1 nm/10 nm) were formed directly on the graphene. (c) Current−luminance characteristics of a single μ-ILED with metal and graphene electrodes. (d) Optical images of μ-ILEDs at different drive currents, with metal (top frames) and graphene (bottom frames) electrodes. (e) Optical microscope images (black and white) showing emission areas corresponding to the results in frame (d). (f) Photographs of an array of 4×6 μ-ILEDs with graphene interconnects, with (top) and without (bottom) external lighting. This device was formed on a glass substrate. The photograph in the right frame highlights the high level of transparency that is possible with graphene interconnects.

expectation as shown in the inset of Figure 2f (see Figure S3b in the Supporting Information for transmittance in the entire visible range). A stacked graphene film with $N_S = 4$ exhibits transparency as high as $T \sim 90\%$ with $R_S \sim 480$ Ω/square.

Figure 3 provides electrical and optical properties of a single μ-ILED with graphene top electrodes ($N_S = 3$), and overall structure shown in Figure 2a. As illustrated in Figure 3a, the μ-ILED with a graphene p-contact and without any Ohmic contact metal, exhibits a turn-on voltage (at $I = 20$ μA) that is $\sim$0.3 V higher and a slope ($\sim 1/R$) that is substantially lower than an otherwise identical μ-ILED with Ohmic metal p-contacts.[7] Measurement of contact resistance with the two-point transmission line method (TLM, optical microscope in the inset of Figure 3b) reveals non-Ohmic behavior of a graphene p-contact as shown in Figure 3b. Despite these nonideal features, the associated optical output power is enhanced with the graphene electrode, as shown in Figure 3c, due to its high level of transparency. For comparison, photographs and optical microscope images of these two types of μ-ILEDs at different drive currents appear in panels d and e of Figure 3, respectively.

Beyond single device demonstrations, graphene used in this manner can interconnect many μ-ILEDs in a scalable fashion, as shown in Figure 3f. The upper and lower images in Figure 3f correspond to a 4×6 array of μ-ILEDs on a glass substrate, driven at a current of 1 mA. The uniform emission characteristics indicate that all devices have similar intimate contacts with graphene and uniform distribution of resistance across the overall system of interconnects.

The right frame of Figure 3f provides a magnified view of the white boxed region in the top frame of Figure 3d, to illustrate the high level of transparency provided by the graphene (see also Figure S5a, Supporting Information). As expected, the current−voltage (I−V) characteristics of such array devices (Figure S5b, Supporting Information) show higher takeoff voltages and lower slopes, compared to those of similar arrays with metal interconnects (Cr/Au, 30/500 nm), due to higher contact and sheet resistances for the graphene case. Graphene films with higher N_S, used in combination with ultrathin metal Ohmic p-contacts, can lead to improvements in these properties.[17]

The favorable mechanics of graphene represent a key advantage over traditional TCOs. To illustrate the compatibility of graphene interconnects with advanced, stretchable forms[18−20] of semiconductor devices, we built arrays of μ-ILEDs interconnected by graphene traces in optimized, noncoplanar serpentine shapes.[21] The shapes and layouts of the interconnects were designed to minimize material strains due to extensional deformations. Details appear in the schematic illustrations of Figure S6 (Supporting Information). Adapted versions of processes and strategies for dual transfer printing[22] can be applied in this case. The designs involve series connections of μ-ILEDs using graphene with photopatterned layers of epoxy on top and bottom in a manner that places the graphene near the neutral mechanical plane.[22] Figure 4a and Figure S7a (Supporting Information) present optical images of a resulting device on a sheet of PDMS ($\sim$400 μm thick). The inset of Figure 4a highlights the non-coplanar characteristics of the serpentine bridges (see also Figure S7b, Supporting Information). The top and bottom
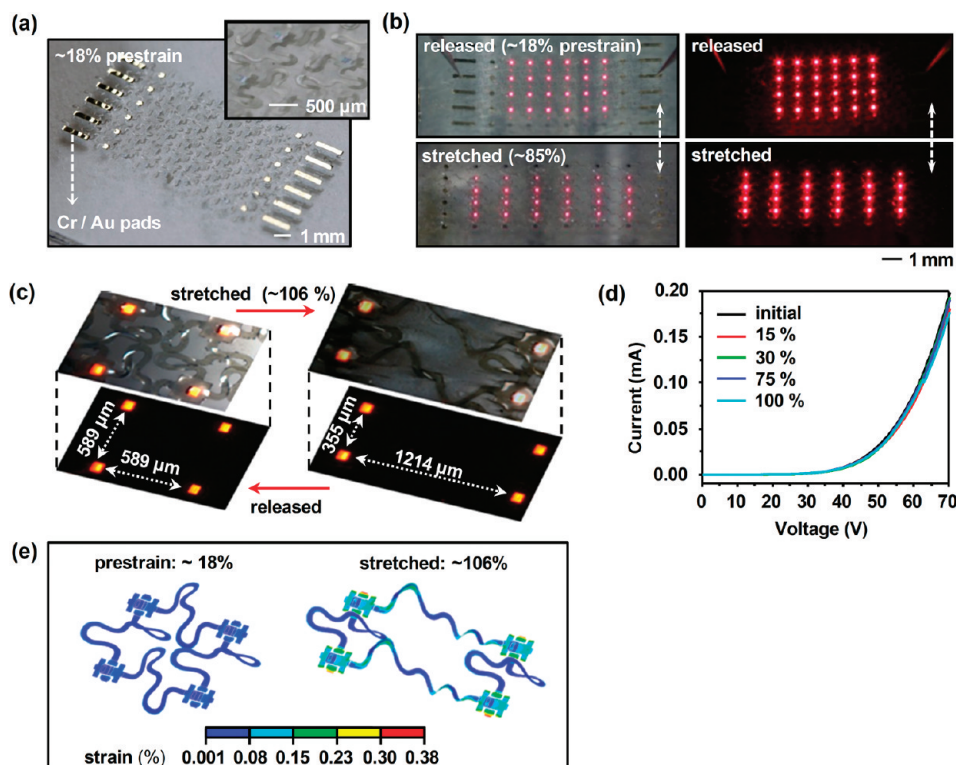
Figure 4. (a) Optical image of a 4 × 6 array of μ-ILEDs with noncoplanar serpentine graphene interconnect bridges on a thin (∼400 μm) slab of PDMS in its off state. The inset provides a magnified view of (a). (b) Optical images of a stretchable 4 × 6 array of μ-ILEDs before (top frame) and after (bottom frame) stretching along the horizontal direction. The left and right frames were collected with and without external lighting, respectively. (c) Optical microscope images of four pixels in a μ-ILEDs array with serpentine graphene interconnects before (left frame) and after (right frame) stretching along the horizontal direction. The top and bottom frames were collected with and without external lighting. (d) Current−voltage characteristics of this array measured in various stretching conditions along the horizontal direction. (e) Strain distributions determined by 3D finite-element model (FEM) for the cases corresponding to frames in (c).

frame of Figure 4b show the device undeformed (∼18% pre-strain) and under uniaxial tensile stretching to a strain of ∼85%, respectively (Movie S1, Supporting Information). Uniform and constant emission characteristics are clearly observable both with (left frame) and without (right frame) external illumination. The maximum stretching before mechanical failure is ∼106%; this limit is shown in the optical microscope images of Figure 4c. No noticeable changes in the $I−V$ characteristics are observed with various stretching conditions up to 100% (Figure 4d), thereby indicating that strains in this range are effectively accommodated by in- and out-of-plane conformational changes in the graphene serpentines, encapsulated by top and bottom layers of epoxy in a manner that avoids any significant deformation of the brittle μ-ILEDs. Additionally, finite element modeling indicates peak strains in the graphene interconnect layer and in the GaAs of active islands were >330 times smaller than the applied strain as shown in Figure 4e. The maximum strains are only 0.049% in graphene and 0.028% in GaAs for applied biaxial prestrain of 18%. For applied external strains of 106% along the horizontal direction, the maximum strains are 0.38% and 0.12% in graphene and GaAs, respectively (see Supporting Information and Figure S8 for details).

In conclusion, this work demonstrates an unusual type of μ-ILED module with graphene interconnects, formed via simple top-down lamination of graphene films onto the structured surfaces of active device arrays. This approach exploits capillarity and generalized adhesion forces to drive conformal contact between the graphene and the devices, in a manner that is compatible with process and design strategies for conventional thin film technologies and stretchable arrays. These attributes suggest the potential for applications in certain existing and emerging uses of LEDs in information display, biomedical devices, and others.

■ ASSOCIATED CONTENT

ⓢ **Supporting Information.** Details about the preparation of CVD-grown graphene, theoretical modeling, Raman spectroscopy of stacked graphene, back gate effect, and FEM simulations. This material is available free of charge via the Internet at http://pubs.acs.org/.

■ AUTHOR INFORMATION

Corresponding Author
*E-mail: jrogers@illinois.edu.

Author Contributions
▽These authors contributed equally.

■ ACKNOWLEDGMENT

■ REFERENCES

(1) Novoselov, K. S.; Geim, A. K.; Morozov, S. V.; Jiang, D.; Zhang, Y.; Dubonos, S. V.; Grigorieva, I. V.; Firsov, A. A. *Science* **2004**, *306*, 666–669.

(2) Li, X.; Cai, W.; An, J.; Kim, S.; Nah, J.; Yang, D.; Piner, R.; Velamakanni, A.; Jung, I.; Tutuc, E.; Banerjee, S. K.; Colombo, L.; Ruoff, R. S. *Science* **2009**, *324*, 1312–1314.

(3) Jo, G.; Choe, M.; Cho, C.-Y.; Kim, J. H.; Park, W.; Lee, S.l; Hong, W.-K.; Kim, T.-W.; Park, S.-J.; Hong, B. H.; Kahng, Y. H.; Lee, T. *Nanotechnology* **2010**, *21*, 175201.

(4) Wu, J.; Agrawal, M.; Becerril, H. A.; Bao, Z.; Liu, Z.; Chen, Y.; Peumans, P. *ACS Nano* **2010**, *4*, 43–48.

(5) Chung, K.; Lee, C.-H.; Yi, G.-C. *Science* **2010**, *330*, 655–657.

(6) Kim, B.-J.; Mastro, M. A.; Hite, J.; Eddy, C. R.; Kim, J. *Opt. Express* **2010**, *18*, 23030–23034.

(7) Park, S.-I.; Xiong, Y.; Kim, R.-H; Elvikis, P.; Meitl, M.; Kim, D.-H.; Wu, J.; Yoon, J.; Yu, C.-J.; Liu, Z.; Huang, Y.; Hwang, K.-C.; Ferreira, P.; Li, X.; Choquette, K.; Rogers, J. A. *Science* **2009**, *325*, 977–981.

(8) Malard, L. M.; Pimenta, M. A.; Dresselhaus, G.; Dresselhaus, M. S. *Phys. Rep.* **2009**, *473*, 51–87.

(9) Koh, Y. K.; Bae, M.-H.; Cahill, D. G.; Pop, E. *ACS Nano* **2011**, *5*, 269–274.

(10) Bae, S.; Kim, H.; Lee, Y.; Xu, X.; Park, J.-S.; Zheng, Y.; Balakrishnan, J.; Lei, T.; Ri Kim, H.; Song, Y. I.; Kim, Y.-J.; Kim, K. S.; Ozyilmaz, B.; Ahn, J.-H.; Hong, B. H.; Iijima, S. *Nat. Nanotechnol.* **2010**, *5*, 574–578.

(11) Huang, Y.; Wu, J.; Hwang, K. C. *Phys. Rev. B* **2006**, *74*, 245413.

(12) Kopesky, E. T.; McKinley, G. H.; Cohen, R. E. *Polymer* **2006**, *47* (1), 299–309.

(13) Xiao, J. L.; Dunham, S.; Liu, P.; Zhang, Y. W.; Kocabas, C.; Moh, L.; Huang, Y. G.; Hwang, K. C.; Lu, C.; Huang, W.; Rogers, J. A. *Nano Lett.* **2009**, *9* (12), 4311–4319.

(14) Li, X.; Zhu, Y.; Cai, W.; Borysiak, M.; Han, B.; Chen, D.; Piner, R. D.; Colombo, L.; Ruoff, R. S. *Nano Lett.* **2009**, *9*, 4359–4363.

(15) Kuzmenko, A. B.; van Heumen, E.; Carbone, F.; van der Marel, D. *Phys. Rev. Lett.* **2008**, *100*, 117401.

(16) Nair, R. R.; Blake, P.; Grigorenko, A. N.; Novoselov, K. S.; Booth, T. J.; Stauber, T.; Peres, N. M. R.; Geim, A. K. *Science* **2008**, *320*, 1308–1308.

(17) Lee, J. M.; Choung, J. W.; Yi, J.; Lee, D. H.; Samal, M.; Yi, D. K.; Lee, C.-H.; Paik, U.; Rogers, J. A.; Park, W. I. *Nano Lett.* **2011**, *10*, 2783–2788.

(18) Lacour, S. P.; Huang, Z.; Suo, Z.; Wagner, S. *Appl. Phys. Lett.* **2003**, *82* (15), 2404–2406.

(19) Lacour, S. P.; Wagner, S.; Narayan, R. J.; Li, T.; Suo, Z. *J. Appl. Phys.* **2006**, *100*, 014913.

(20) Lacour, S. P.; Chan, D.; Wagner, S.; Li, T.; Suo, Z. J. *Appl. Phys. Lett.* **2006**, *88*, 204103.

(21) Kim, D.-H.; Song, J.; Choi, W. M.; Kim, H.-S.; Kim, R.-H.; Liu, Z.; Huang, Y. Y.; Hwang, K.-C.; Zhang, Y.; Rogers, J. A. *Proc. Natl. Acad. Sci. U.S.A.* **2008**, *105* (48), 18675–18680.

(22) Kim, R.-H.; Kim, D.-H.; Xiao, J.; Kim, B. H.; Park, S.-I.; Panilaitis, B.; Ghaffari, R.; Yao, J.; Li, M.; Liu, Z.; Malyarchuk, V.; Kim, D. G.; Le, A.-P.; Nuzzo, R. G.; Kaplan, D. L.; Omenetto, F. G.; Huang, Y.; Kang, Z.; Rogers, J. A. *Nat. Mater.* **2010**, *9*, 929–937.

Stretchable, Transparent Graphene Interconnects for Arrays of Microscale Inorganic Light Emitting Diodes on Rubber Substrates

Rak-Hwan Kim[1,⊥], Myung-Ho Bae[2,⊥], Dae Gon Kim[1], Huanyu Cheng[3], Bong Hoon Kim[1,4], Dae-Hyeong Kim[1], Ming Li[3,5], Jian Wu[3], Frank Du[1], Hoon-Sik Kim[1], Stanley Kim[1,2], David Estrada[2], Suck Won Hong[6], Yonggang Huang[3], Eric Pop[2], and John A. Rogers[1,*]

[1]Department of Materials Science and Engineering, Beckman Institute for Advanced Science and Technology and Frederick Seitz Materials Research Laboratory, University of Illinois at Urbana-Champaign, Urbana, IL 61801 USA

[2]Department of Electrical and Computer Engineering, Micro and Nanotechnology Laboratory, University of Illinois at Urbana-Champaign, Urbana, IL 61801 USA

[3]Department of Mechanical Engineering and Department of Civil and Environmental Engineering, Northwestern University, Evanston, IL 60208

[4]Department of Materials Science and Engineering, Korea Advanced Institute of Science and Technology (KAIST), Daejeon, 305-701, Korea

[5]State Key Laboratory of Structural Analysis for Industrial Equipment, Dalian University of Technology, Dalian 116024, People's Republic of China

[6]Department of Nanomaterials Engineering, Pusan National University, Miryang, 627-706, Korea

[*]To whom correspondence should be addressed.   E-mail: jrogers@illinois.edu

[⊥]These authors contributed equally.

.

Supplementary Information

Preparation of CVD-grown graphene

We grew graphene by chemical vapor deposition (CVD). A 50 µm thick Cu foil (provided by Alfa Aesar) wrapped around a quartz rod was inserted into a quartz reaction tube (1 inch diameter) and then heated to 1000 °C at a ramp speed of 24 °C/min under flowing hydrogen gas, where the pressure of the tube is kept at 0.26 Torr. After flowing a reacting gas mixture (CH_4:H_2=850:50 sccm) for 30 min under 2.6 Torr, the sample was cooled to room temperature with a rate of 20 °C/min. The pressure was increased to ambient when the temperature reached 200 °C. Figure S1a shows the experimental sequence. The graphene grows on both the top and bottom surfaces of the copper foil. Typically, we removed the graphene from one side by oxygen plasma etching with the other protected with a PMMA layer (see Fig. S1b). The foil was then placed in a 1M aqueous solution of $FeCl_3$ to eliminate the copper. After ~10 hours, the floating graphene with PMMA was transferred to deionized (D.I.) water to wash out the etchant and to prepare the film for lamination on the LED substrate.

Theoretical modeling

The graphene (or PMMA) layer is modeled as beam to form conformal integration onto the p and n-contact regions. The sagging profile w is characterized by the sagging height h and un-contacted length a to be determined, as shown in Fig S2. The boundary conditions for the deflection and rotation are $w = 0$ and $w' = 0$ at $x = 0$, and $w = h$ and $w' = 0$ at

$x = a$, which give the sagging profile $w = 3h(x/a)^2 - 2h(x/a)^3$. The total energy U is

the sum of potential energy and bending energy as $U = -\gamma(L - 2a) + 12(EIh^2/a^3)$, where

γ is the work of adhesion between graphene and GaAs, and EI is flexural rigidity of

graphene. Energy minimization $dU/da = 0$ gives $a = (18EIh^2/\gamma)^{1/4}$, and the total energy

$U_{min} = 48(EIh^2)^{1/4}(\gamma/18)^{3/4} - \gamma L$. Sagging requires that U_{min} be smaller than the energy

of unsagged state (zero), which gives critical condition for sagging as

$EIh^2/(\gamma L^4) < 9/8192$. It leads to Eq. (1) within one percent error. The contact coverage

of graphene layer is defined by $P = (L - 2a)/L = 1 - 2[18EIh^2/(\gamma L^4)]^{1/4}$.

Raman spectroscopy of stacked graphene films

Figure S3a shows the Raman spectra for various number of stacked graphene films. For

N_S=1, the 2D and G bands are found at ~2646 cm^{-1} and ~1587 cm^{-1}, respectively with

I(G)/I(2D) ~ 0.2, indicating monolayer graphene.[1,2] For N_S=2, and N_S=4, similar

monolayer signatures appear, i.e. I(G)/I(2D)=0.23 and 0.14, respectively.[3] We note there

is an important distinction between the I(G)/I(2D) ratio of graphene films obtained after

multiple transfers[3] vs. the as-grown or exfoliated multilayer graphene.[1,2] After multiple

transfers the I(G)/I(2D) ratio does not change substantially (remaining <0.5) because the

transferred layers are randomly stacked and behave independently.[3] For as-grown or

exfoliated multilayers, the I(G)/I(2D) ratio increases with N_S, see e.g. Fig 27 in Ref. [1], or

Fig 1b in Ref [2]. We do note some red shifting of the 2D bands after multiple transfers,

consistent with reports by Bae et al.[3]   For instance, the position of the 2D band moves

from 2645 cm^{-1} for N_S=1 to 2655 cm^{-1} for N_S=4.   This shift could indicate hole doping

from the multiple transfers, possibly due to trapped water and oxygen between the graphene

layers.[4,5]   The intensities of both G and 2D bands increase with N_S after multiple transfers

(but their ratio remains approximately unchanged as stated above).

Mobility of graphene device

Figure S4 shows the drain current as a function of back-gate voltage (I_D-V_{GD} curve)

measured in vacuum (~4×10^{-5} Torr) at room temperature.   The same four probe geometry

with channel length (L) and width (W) of 28 μm and 10 μm respectively, was used with a

typical single layer graphene device.   The results show a local minimum current at

V_{GD}=0V when the Fermi level crosses the Dirac point.   The slope of the curve shows a

asymmetric behavior with respect to V_{GD}=0V, similar to other reports.[6]   The field-effect

mobility is μ = (dI_D/dV_{GD}) × [L/(WC_iV_{GD}], where C_i is the SiO$_2$ capacitance per unit area,

and we obtain μ ~ 2000 and ~360 cm^{2}V^{-1}s^{-1} for holes and electrons, respectively.   Here,

dI_D/dV_{GD} for each doping state was obtained from the slopes of the red lines on the data

points in Fig. S4.

FEM simulation

Finite Element Analysis (FEA) is used to study the deformation of graphene, GaAs, and

epoxy layers in interconnects and devices.   The PDMS substrate (thickness 400 um,

Young's modulus 2 MPa and Poisson's ratio 0.48) is modeled by 3D solid stress element

C3D8R in the ABAQUS finite element program[7] since its thickness is much larger than interconnects and devices (~5 µm). Interconnects and devices are modeled by (composite) shell element S4R since they are multilayer structures. Uniform displacements are applied on the left and right surfaces of PDMS to simulate pre-strain and stretching deformations. The peak strains in top and bottom encapsulation layers are shown in Fig S7.

SI Reference

[1] Malard, L.M.; Pimenta, M.A.; Dresselhaus, G.; Dresselhaus, M.S. *Phys. Reports* **2009,** 473, 51-87.

[2] Koh, Y. K.; Bae, M.-H.; Cahill, D. G.; Pop, E. *ACS Nano* **2011**, 5, 269-274.

[3] Bae, S.; Kim, H.; Lee, Y.; Xu, X.; Park, J.-S.; Zheng, Y.; Balakrishnan, J.; Lei, T.; Ri Kim, H.; Song, Y. I.; Kim, Y.-J.; Kim, K. S.; Ozyilmaz, B.; Ahn, J.-H.; Hong, B. H.; Iijima, S. *Nature Nano.* **2010**, 5, 574-578.

[4] Das, A; Pisana, S; Chakraborty, B; Piscanec, S; Saha, S. K.; Waghmare, U.V.; Novoselov, K. S.; Krishnamurthy, H. R.; Geim, A. K.; Ferrari, A. C.; Sood, A. K. *Nat Nano* **2008,** 3, 210-215.

[5] Wehling, T. O.; Lichtenstein, A. I.; Katsnelson, M. I. *Applied Physics Letters* **2008**, 93, 202110.

[6] Huard, B.;Stander, N; Sulpizio, J.A & Goldhaber-Gordon, D. *Phys. Rev. B* **2008**, 78, 121402(R).

[7] ABAQUS Analysis User's Manual V6.9 (Dassault Systèmes, Pawtucket, RI, **2009**).

SI Figure captions

Figure S1. Schematic illustrations of fabrication procedures for the downside contact of a graphene film, grown on a sheet of Cu.

Figure S2. Schematic illustration of the theoretical modeling used to study sagging mechanisms of graphene films into relief features.

Figure S3. Raman spectroscopy (a) and transmittance (b) of films with different numbers of graphene layers N_s (= 1, 2, and 4) after multiple layer transfers.

Figure S4. Drain currents from a patterned single layer graphene film as a function of back-gate voltage (I_D-V_{GD} curve) measured in a vacuum at room temperature.

Figure S5. (a) Optical images of a 4×6 array of μ-LEDs with graphene interconnects in its off state. (b) Current-voltage characteristics of an array of 4×6 μ-ILEDs with metal (Cr/Au, 30/500 nm) and graphene (3 layers) interconnects, respectively.

Figure S6. Schematic illustration of 4×6 array of μ-ILEDs with serpentine graphene interconnect bridges (top) and its magnified view which is providing design strategy in details (bottom).

Figure S7. (a) Optical image of a 4×6 array of μ-ILEDs with non-coplanar serpentine graphene interconnect bridges on a thin (~400 μm) slab of PDMS in its light on states. (b) Optical image of a 4×6 array of μ-LEDs on a thin (~400 μm) slab of PDMS substrate, which was transfer printed without prestrain (top), and its enlarged view (bottom).

Figure S8. Strain distributions of top and bottom epoxy layers, determined by 3D-FEM for the cases corresponding to frames in Fig. 4c.

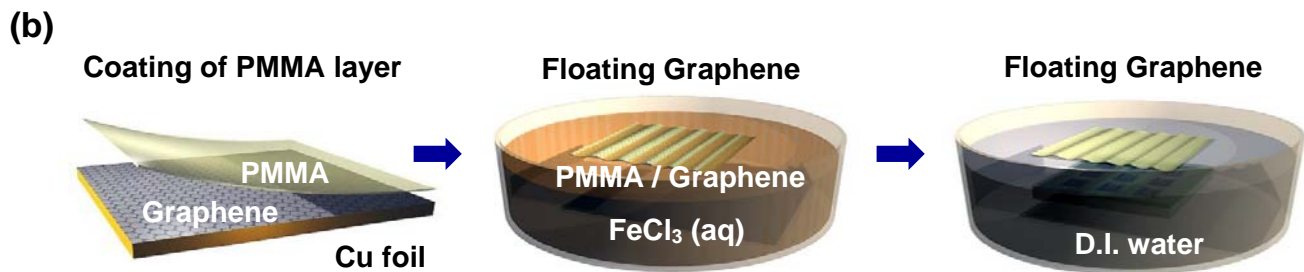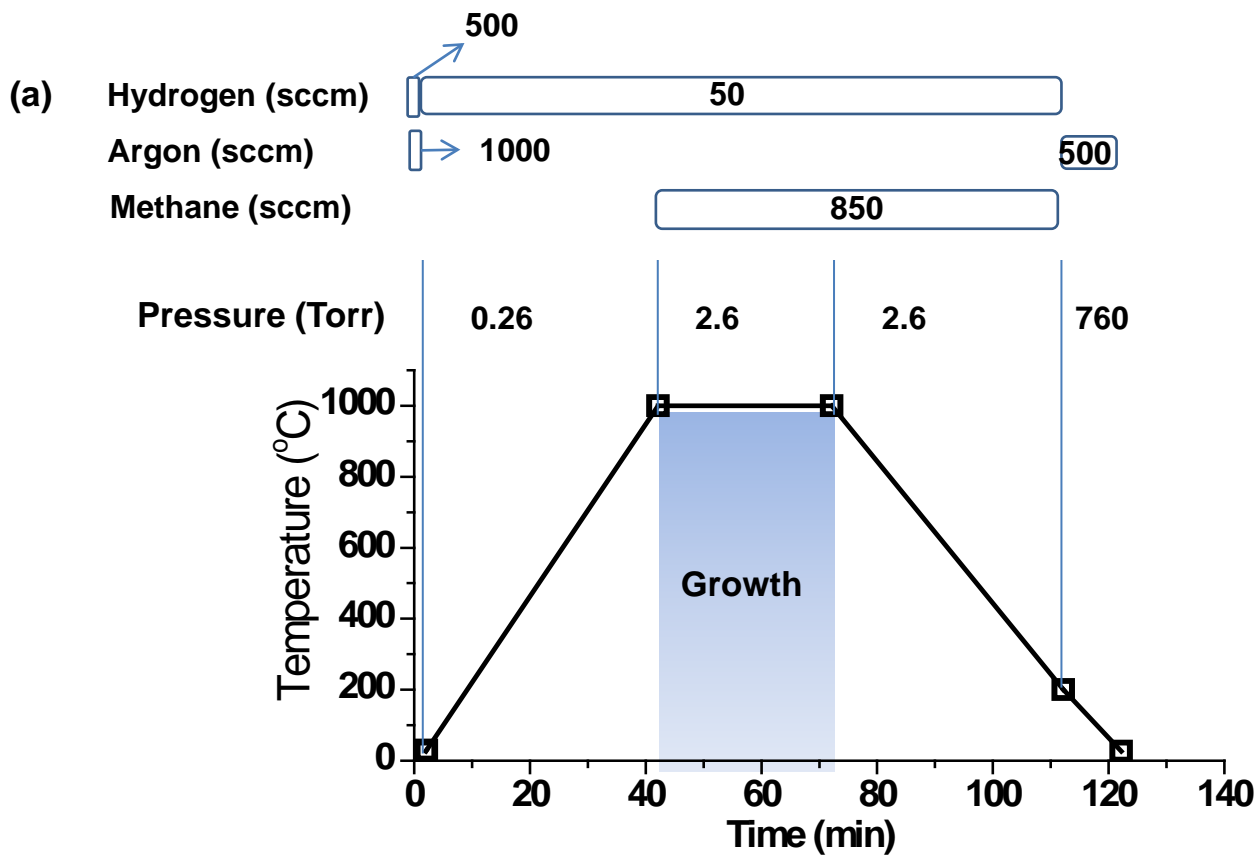**Movie S1.** 3D FEM simulation of stretchable LEDs array.

(a)
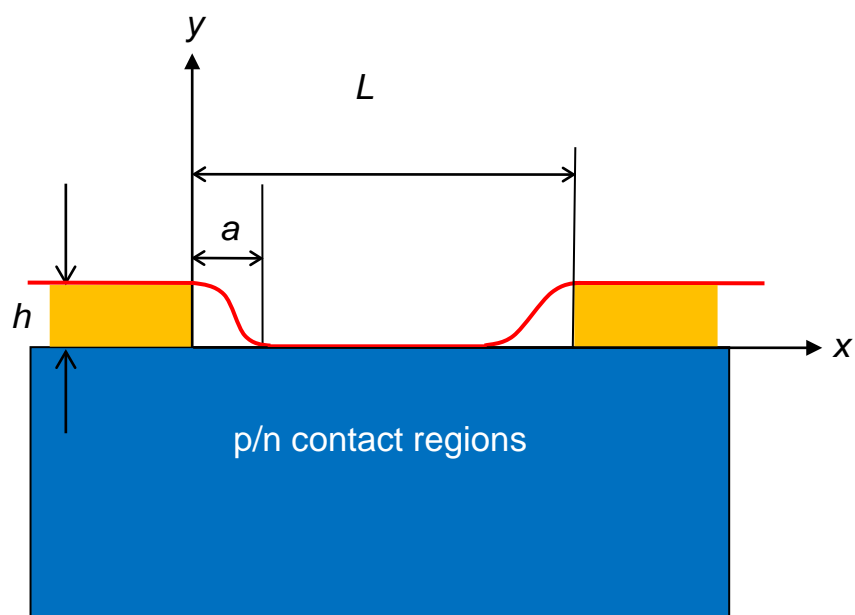
Hydrogen (sccm)	500	50
Argon (sccm)	1000	500
Methane (sccm)		850

Pressure (Torr) 0.26   2.6   2.6   760

Growth

(b)

Coating of PMMA layer

PMMA
Graphene
Cu foil

Floating Graphene

PMMA / Graphene
FeCl$_3$ (aq)

Floating Graphene

D.I. water

Figure S1

Figure S2

(a)

stacked number
— 1
— 2
— 4

2D

G

D

(b)

stacked number
— 1
— 2
— 4

Figure S3

Figure S4

(a) graphene electrode — 1 mm

printed μ-ILEDs

(b)

metal Electr.
graphene Electr.
($N_s = 3$)

Figure S5

Connected in series

697 μm

280 μm

Polymer for encapsulation

Graphene interconnects

50 μm

70 μm

printed μ-ILED

Figure S6

(a)

— 1 mm

(b)

no prestrain (on elastomer)

—1 mm

——200 μm

Figure S7

(a)

strain (%)

0.001 0.015 0.30 0.45 0.60 0.75

strain (%)

0.01 0.7 1.4 2.1 2.8 3.5

(b)

strain (%)

0.001 0.13 0.26 0.39 0.42 0.65

strain (%)

0.01 1.0 2.0 3.0 4.0 5.0

Figure S8

PDMS

Movie S1